Article
Vol. 24, No. 4, p. 407–424, August 2020
https://doi.org/10.1007/s12303-019-0030-y
pISSN 1226-4806 eISSN 1598-7477
Geosciences Journal GJ

Geological and mineralization characteristics of the Kestanelik epithermal Au-Ag deposit in the Tethyan Metallogenic Belt, NW Turkey

Nilay Gülyüz[1,2]*, Erhan Gülyüz[2], Zoe K. Shipton[1], İlkay Kuşcu[3], and Richard A. Lord[1]

[1]Department of Civil and Environmental Engineering, Faculty of Engineering, University of Strathclyde, Glasgow, G1 1XJ, UK
[2]Department of Geological Engineering, Faculty of Engineering, Van Yüzüncü Yıl University, Van 65080, Turkey
[3]Department of Geological Engineering, Faculty of Engineering, Muğla Sıtkı Koçman University, Muğla 48000, Turkey

ABSTRACT: Kestanelik epithermal gold deposit is situated in the Biga Peninsula, which hosts numerous metallic deposits belonging to the Tethyan Metallogenic Belt. In the Biga peninsula the Tethyan Metallogenic Belt is represented by a Neo-Tethyan suture zone. Discovered deposits along the belt are commonly associated with Cenozoic magmatism ranging between 52 and 18 Ma in age, formed due syn- to post-collisional tectonics. In this study, we focus on the deposit-scale geological and mineralization characteristics of Kestanelik in order to determine the formation and evolution of the deposit within the tectono-magmatic history of the Biga Peninsula. We (1) mapped the geology of the deposit area (2) conducted paleostress analyses, (3) observed and examined the macroscopic and petrographical textural, mineralogical and alteration characteristics of the mineralization and (4) interpreted geophysical resistivity survey and geochemical assay data. The stratigraphic age of the Kestanelik deposit, bracketed by cross cutting relations and supported by the geophysical data, is middle Lutetian–early Priabonian which also implies that the deposit has a genetic link with the Cenozoic post-collisional calc-alkaline magmatism. A NE-SW oriented compressional regime determined from the paleostress analyses is consistent with the kinematics of the vein system and is attributed to the collision and further convergence after the closure of the northern branch of the Neo-Tethys Ocean. The fracture system provided structural pathways for the transport of the hydrothermal fluids. The common presence of pseudo-bladed quartz and hydrothermal breccias, and the low total sulphide and base metal contents in the mineralized veins indicate that the Kestanelik is a low sulphidation epithermal-type gold deposit. Boiling, mixing (hypogene oxidation) and supergene enrichment are the likely gold deposition and enrichment processes respectively.

Key words: epithermal, gold, mineralization, Biga Peninsula, Tethyan Metallogenic Belt

Manuscript received May 1, 2019; Manuscript accepted August 26, 2019

1. INTRODUCTION

The Biga Peninsula forms the northwestern part of the Anatolian Peninsula where numerous microcontinents collide. The main components are the Anatolide-Tauride Block (ATB) in the south belonging to Gondwana, and the Pontides in the north belonging to Laurasia. The Biga Peninsula is tectonically located at the south-westernmost tip of the Pontides at the boundary between Gondwana and Laurasia (Fig. 1a). It has long been known as an important part of the Tethyan Metallogenic Belt (TMB) (or Alpine-Himalayan Belt) and the region has been the focus of gold exploration and mining since the ancient times from Lydians, Greeks, Romans, and Ottomans to the present-day. Many economic porphyry and epithermal (high-, low- and intermediate-sulphidation) ore deposits have been discovered in the region such as Halilağa, Ağı Dağı, Kirazlı, Kartaldağ and Madendağ (Yiğit, 2009; Yiğit, 2012; Ünal-İmer et al., 2013). The deposits are spatially associated with shallow-level acidic to intermediate plutonic and volcanic rocks which are genetically linked with Cenozoic calc-alkaline magmatism in the region (Yiğit, 2012). The Kestanelik epithermal gold deposit is one of the important ore deposits discovered by Eurogold Madencilik Incorporated in 1992, it was taken over by Chesser Resources in 2009 and has been operated as an active mine by Tümad Madencilik Incorporated since November 2017. It is located 45 km NE of Çanakkale and hosted by mica schist and quartz-

*Corresponding author:
Nilay Gülyüz
Department of Geological Engineering, Faculty of Engineering, Van Yüzüncü Yıl University, Van 65080, Turkey
Tel: +90-535-244-17-20, E-mail: nilaygulyuz@yyu.edu.tr

feldspar-hornblende (QFH) porphyry. Previous studies on the epithermal gold mineralization at Kestanelik consist of unpublished company reports which generally compile drillhole, rock and soil geochemical assay data to suggest drilling locations. All of them lacked a detailed tectonic context to understand the geological story of the mineralization. A recent study by Gülyüz et al. (2018) presented the permeability enhancement mechanisms of the Kestanelik vein system by focusing on the dimensions, geometry, kinematics, textures and breccias of the veins.

The main aim of the current paper is to place the local geological history of the Kestanelik epithermal gold deposit within the regional tectono-magmatic context. In addition, understanding the mineralogical, textural and alteration characteristics of the gold mineralization is attempted. A review of the complex geology of the Biga Peninsula based on the compiled literature data is followed by a summary of the general structural characteristics of the mineralized veins. The results of this investigation are then presented as (1) the geology of the study area, together with a detailed geological map of the units exposed in the deposit area and its mineralized veins, (2) a generalized tectono-stratigraphic section of the area, (3) structures in the area and kinematic analyses of fault slip data, and (4) general characteristics of the mineralization and alteration.

2. BACKGROUND

2.1. Geological Background of the Biga Peninsula

The geological evolution of Turkey has mainly been controlled by the relative movement of the Eurasian, African and Arabian plates during the closure of the Paleo- and Neo-Tethys oceans. The boundaries of these plates in Turkey are represented by two main suture zones, which can be considered as parts of the Alpine-Himalayan orogenic belt. These suture zones are the İzmir-Ankara-Erzincan suture zone (İAESZ) (between the Eurasian and the African plates) in the north, and the Bitlis-Zagros suture zone (BZSZ) (between the African and the Arabian plates) in the south (Fig. 1a; Şengör and Yılmaz, 1981). Today's mosaic geometry of Turkey is explained by the amalgamation and/or juxtaposition of multi-rooted continental and oceanic fragments during orogenic processes.

The Biga Peninsula in NW Turkey is characterized by juxtaposition of two main tectonic blocks: the Anatolide-Tauride Block (ATB) (African) in the south and the Pontides (Eurasia) in the north (Fig. 1a).

Cenozoic magmatic rocks together with marine and continental sedimentary rocks dominate the geology of the Biga Peninsula, whereas pre-Cenozoic metamorphic and ophiolitic rocks constitute the regional basement (Fig. 1b).

Records of pre-Cenozoic tectonic events in the Biga Peninsula are only observed in the basement rocks including metamorphic complexes and slivers of NE-SW trending ophiolites or ophiolitic mélanges (Fig. 1b). The formation and evolution of these rocks are related to the evolution of Paleo-Tethys and early stages of the Neo-Tethys Oceans (Okay et al., 1996; Okay and Satır, 2000a). Cenozoic evolution of the region is accompanied by the generation of numerous epithermal and porphyry-Cu type deposits, hosted not only by the basement rocks but also by the Cenozoic

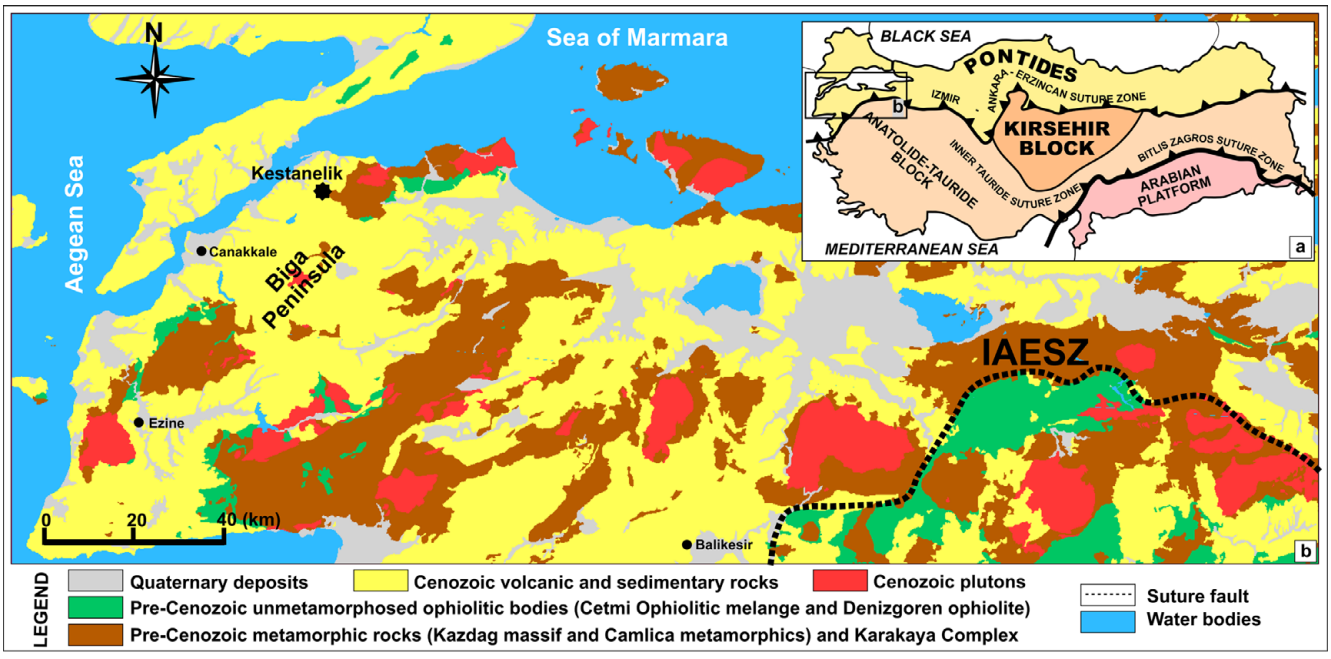

Fig. 1. (a) Major tectonic divisions of Turkey (simplified from Okay and Tüysüz, 1999). (b) Simplified geological map of the Biga Peninsula (IAESZ: İzmir-Ankara-Erzincan Suture Zone) with the location of the study area Kestanelik (modified from Turkecan and Yurtsever, 2002).

magmatic and sedimentary rocks. The Cenozoic period is marked by four major tectonic events, from oldest to the youngest: (a) closure of the Neo-Tethys Ocean by northward subduction, (b) continental collision along the İAESZ, (c) post-collisional tectonism and (d) subduction along the Hellenic Trench beneath Anatolia and westward escape of the Anatolian plate (neotectonic period). Traces of these events are observed in the basement rocks and allow the timing of the major tectonic events in the region to be constrained.

The Neo-Tethyan subduction is marked by HP–LT metamorphism of the Paleozoic Çamlıca metamorphics based on relics of eclogites. Three muscovite samples from quartz mica schists give 69 to 65 Ma Rb/Sr ages (Okay and Satır, 2000b) indicating Maastrichtian regional metamorphism. Additionally, biostratigraphic ages determined from the radiolarites and limestone blocks of the Çetmi Ophiolitic mélange overthrusting the Çamlıca metamorphics vary between Early Triassic–Late Cretaceous (Okay et al., 1990; Beccaletto et al., 2005). This interval marks the termination of the mélange formation and subsequent commencement of the continental collision along the İAESZ. Timing of the collision along the İAESZ, while still not certain, is proposed as Late Cretaceous–Early Eocene (Şengör and Yılmaz, 1981; Harris et al., 1994; Okay and Tüysüz, 1999; Sherlock et al., 1999; Önen and Hall, 2000; Hinsbergen et al., 2010). Evidence of post-collisional events are shown by the geochemical signatures of the Eocene to middle Miocene magmatic rocks (e.g., Altunkaynak and Genç, 2008), although Cenozoic magmatism in the region continued by the Quaternary. After the middle Miocene, the geochemistry of the magmatic rocks shifts to alkaline and this abrupt transition is attributed to thinned crust and asthenospheric upwelling due to advanced extensional tectonics caused by north-dipping subduction along the Hellenic trench (Dilek and Altunkaynak, 2006; Altunkaynak and Genç, 2008), which likely commenced in the middle Miocene (12–11 Ma) (McKenzie, 1978; LePichon and Angelier, 1979; Meulenkamp et al., 1988). This time interval is also supported by early to middle Miocene (20–10 Ma) exhumation ages of the oldest metamorphic complex, the Kazdağ Massif, based on the apatite fission track dating study of Cavazza et al. (2009), who relates these ages to the back-arc extension resulting from slab roll-back in the Hellenic subduction system. The N-S-directed extensional tectonic regime related to the subduction is coupled with strike-slip deformation of the E-W-oriented North Anatolian Fault Zone (NAFZ). This coupling causes a transtensional regime which is represented by the NE-SW-oriented transtensional splays of the NAFZ in the Biga peninsula (e.g., Bozkurt, 2001).

2.2. General Characteristics of the Mineralized Vein System

Gold mineralization in the Kestanelik deposit is hosted by quartz veins/breccia bodies widely exposed over an area of nearly 2 km^2 (Gülyüz et al., 2018). They are hosted by mica schist and quartz-feldspar-hornblende (QFH) porphyry (Fig. 2a). There are nine major mineralized quartz veins/breccias; these are from north to south, named as the Karatepe, KK4, KK3, KK2, KK1,

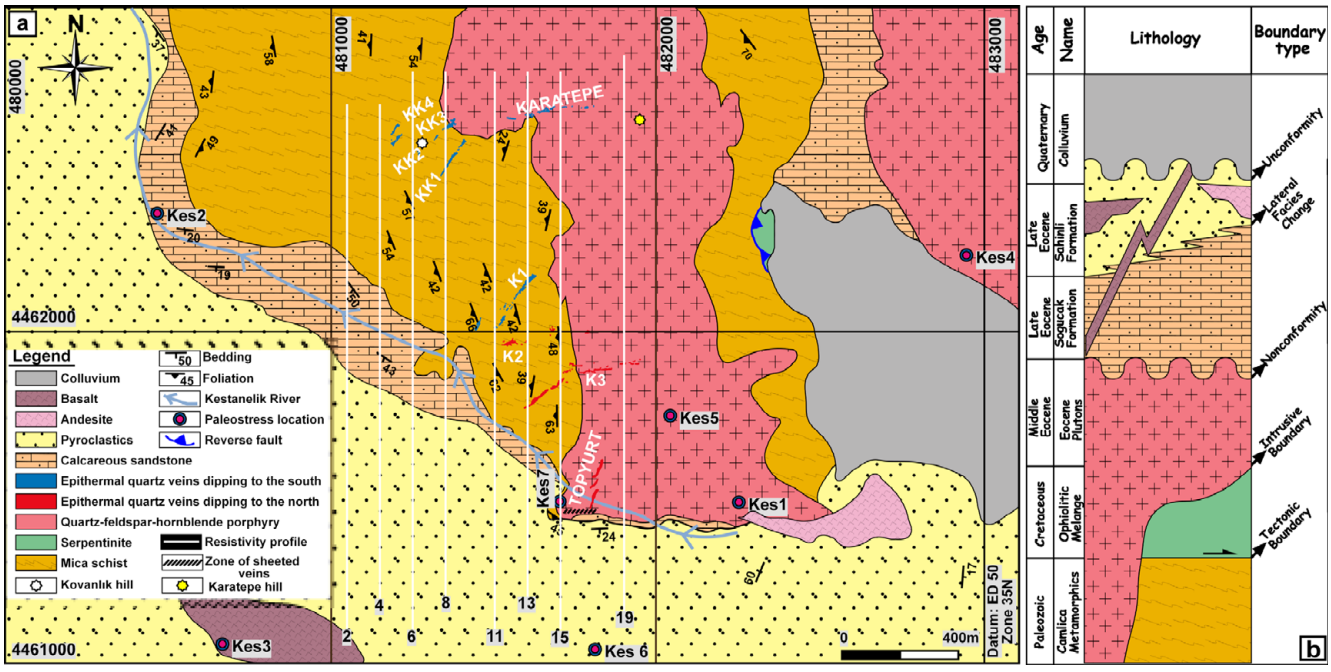

Fig. 2. (a) Geological map of the study area Kestanelik deposit with paleostress locations and resistivity profiles (modified from Gülyüz et al., 2018). (b) Generalized tectono-stratigraphic section of the Kestanelik area.

https://doi.org/10.1007/s12303-019-0030-y

K1, K2, K3, and Topyurt veins. The veins generally have lengths of several tens to several hundreds of meters and their widths vary between 0.8 and 13.6 m on the surface. Based on their attitudes, mineralized veins/breccias are grouped into two sets: E-W-trending ones (Karatepe, K2 and K3E veins) and NE-SW ones (KK1, KK2, KK3, KK4, K1, K3W and Topyurt veins). While the Karatepe, K3E and Topyurt veins are hosted by QFH porphyry, the others are hosted by mica schist. The K3 vein is composed of two segments of different orientations hosted by two different host rocks (Fig. 2a). The margins of the major quartz veins/breccias have transitional lateral boundaries from the main quartz lodes through comb textured extensional wall rock quartz veins and veinlets to hydrothermally-altered host rock. In addition to the mineralized major veins and wall rock veins; sub-vertical and sub-parallel mineralized sheeted quartz veins are observed along the valley floor of the Kestanelik River (Gülyüz et al., 2018; Fig. 2a).

Detailed structural and textural data collected from the outcrop and drill core samples has led to a better understanding of the origin of the fractures hosting the epithermal veins and the kinematics of the vein system at Kestanelik. According to the paleostress analysis on the vein geometries (Gülyüz et al., 2018), the inferred orientations of principal stresses σ_1, σ_2 and σ_3 acting on the mineralized vein system at the time of mineralization are estimated as 034°/02°, 124°/59° and 304°/31° respectively. The N35°W direction of the horizontal component of σ_3 obtained by plotting the strikes of the all extensional veins in the area is consistent with the orientation of σ_3, indicating that all vein structures were controlled by a sub-horizontal NE-SW-oriented σ_1 at the time of mineralization. The inferred direction of the principal stresses together with (1) the wall rock deformation and (2) textural and breccia characteristics of the veins indicate that the E-W-trending Karatepe, K3, and K2 veins are left-lateral strike-slip faults, while the NE-SW-trending KK1, KK2, KK3, KK4, and K1 veins are extensional (Mode I) fractures. In addition, the NE-SW-trending Topyurt vein and associated wall-rock veins correspond to a right-lateral en-echelon brittle shear zone (Gülyüz et al., 2018).

3. STUDIED MATERIALS AND METHODOLOGY

3.1. Data Supplied by License Holder at the Time of Study

The data supplied by Chesser Resources for this study include: (1) collar, survey and assay data of 255 diamond cut and 141 reverse circulation (RC) drill holes, (2) geochemical assay data of vein rock samples, and (3) geophysical resistivity survey data collected from eight N-S-directed lines traversing the mineralized area.

3.2. Geological Mapping

Due to the steep topography of the area and the thick soil cover, natural outcrops were mainly observed on the valley floor. There were also multiple artificial outcrops where drill pads were sited. For the purpose of geological mapping of an area covering approximately 6 km^2, all accessible areas were walked and notes recorded about the rock units and the lithological boundaries. Photos were taken from key locations (well exposed examples of the lithological units, lithological boundaries etc.). Attitudes of foliations and bedding planes were measured using a Brunton geological compass. Point data (x,y,z) were collected from locations of lithological units, boundaries, strike and dip data using a Garmin GPS. These point data (438 points) and the entry lithology of all drill holes (both diamond cut and reverse circulation (RC) holes) (397 points) provided by Chesser Resources were then used to prepare the revised geological map (Fig. 2a) using GIS software Global Mapper, Google Earth, and drawing software Freehand MX.

3.3. Paleostress Analyses

Attitude data, rake of slickenlines, and sense of slip (using surface geometry and/or offsets) were recorded from small–scale fault planes. In total 69 fault-slip data were collected from 7 locations (Fig. 2a) and used for paleostress analyses in order to determine the local deformation phase(s) in the area.

Determining the most coherent stress tensors of slips that occurred on fault surfaces is the main aim of paleostress analyses. This inverse solution is overcome by various proposed methods (e.g., Angelier, 1979; Etchecopar et al., 1981; Armijo et al., 1982; Hardcastle, 1989). All of the methods assume: (1) the direction of maximum shear stress is parallel to the direction of movement on the fault plane, (2) the movement along the fault plane is independent from the movement on the other faults, (3) there is no rotation of the block bounded by the fault planes, and (4) the stress field responsible for the movements on the fault planes is independent of the faults and homogenous. With these assumptions, paleostress inverse solution is easily applied for homogeneous fault systems (e.g., Angelier, 1979, 1989, 1994; Nemcok et al., 1999). However, fault systems in reality are generally not homogeneous and may form under the effect of several different stress regimes. In this case, combinations of homogeneous subsystems are used for artificially determining heterogeneous fault systems (Angelier, 1989). The stress field in the Kestanelik area was expected to be heterogeneous due to possible effects of both escape tectonics caused by the collision of Arabian and Anatolian plates in southeastern Turkey and the extensional tectonics caused by back-arc opening along the Hellenic trench in the Aegean Sea at

the south of Western Turkey. The Gauss method of Zalohar and Vrabec (2007) is useful for separating heterogeneous fault systems into the homogenous fault subsystems. The T-TECTO 3.0 software package, based on the Gauss method (Zalohar and Vrabec, 2007), was therefore used for paleostress analyses of the fault-slip data collected from the study area. The parameters used in the calculation are given below and detailed explanations of their calculations are given in Zalohar and Vrabec (2007).

Dispersion parameter (s) describing angular misfits between the actual and calculated direction of slip along the fault was taken as 20° for this study in order to discard possible irrelevant data.

Compatibility measure (parameter d) calculated by considering the misfit angle between actual and predicted direction of movement on the fault. In this study, it was chosen as 30° due to the high possibility of having a moderately heterogeneous stress field.

Parameter q1 and q2: (q1) roughly represents the internal friction angle of an intact rock which will be fractured whereas (q2) defines the maximum residual frictional angle for activating pre-existing fractures. In this study, (q1) and (q2) were taken as 60° and 20°. This allows the consideration of possible re-activated fractures or intact rocks having different internal friction angles because there are different rock types hosting the faults in the study area.

Orientation of the σ_1 (maximum), σ_2 (intermediate), and σ_3 (minimum) principal stress axes, and the shape ratio of the principal stress differences ($\Phi = (\sigma_2 - \sigma_3)/(\sigma_1 - \sigma_3)$) are the main findings of paleostress inversion solutions. The basic stress regimes are, (a) extensional regimes described by almost vertical σ_1, (b) strike-slip by almost vertical σ_2 and (3) compressional regimes by almost vertical σ_3. In addition to these pure regimes, intermediate regimes (trans-tensional, transpressive, radial-extensional or radial-compressional) also exist. Delvaux et al. (1997) defines these intermediate regimes by a numeric index (Φ') calculated from (Φ) ($\Phi' = \Phi$, where σ_1 is close to vertical; $\Phi' = 2 - \Phi$ where σ_2 is close to vertical; $\Phi' = 2 + \Phi$ where σ_3 is close to vertical).The different stress regimes characterized by different Φ' values are; radial extension ($0 < \Phi' < 0.25$), pure extension ($0.25 < \Phi' < 0.75$, trans-tension ($0.75 < \Phi' < 1.25$), pure strike-slip ($1.25 < \Phi' < 1.75$), transpression ($1.75 < \Phi' < 2.25$), pure compression ($2.25 < \Phi' < 2.75$) and radial-compression ($2.75 < \Phi' < 3$).

3.4. Macroscopic Examination of Mineralized Veins and Examination of Geochemical Assay Data

Macroscopic studies were conducted on (1) textures and breccias of the mineralized epithermal veins and (2) vein and alteration minerals on the outcrop and in drill cores. Geochemical assay data obtained from drill cores and vein rock samples supplied by Chesser Resources were also examined. These data helped us to understand the general mineralogical, textural, and alteration properties of the mineralization.

3.5. Petrographical Analyses

Surface and drill core samples for the purpose of thin section preparation were collected from three well-exposed key veins which represent gold mineralization in different parts of the study area: Karatepe, KK1 and K3 veins. Petrographical analyses were performed from 57 thin sections in total (6 sections from the Karatepe vein, 20 sections from the KK1 vein, and 31 sections from the K3 vein). Examination of the sections sheds more light on the mineralogical and textural characteristics of the mineralized veins.

3.6. Geophysical Resistivity Survey Data

A geophysical resistivity survey with a pole-dipole array was conducted by Zeta for Chesser Resources in May 2010. The survey was conducted along eight N-S-oriented profiles varying in length between 1200 and 1700 meters (Fig. 2a). Spacing between the profiles is not consistent and varies between 50 and 200 meters. The first current electrode was located 250 m south from the southern tip of the profiles and the unit electrode spacing was 25 and 50 meters for 1 to 5 and 6 to 8 levels respectively. Resistivity data were collected from the electrodes multiple times and the data that had the smallest standard deviation value, implying highest quality, were compiled and modelled using RES2DINV software. 2D resistivity sections were constructed by Zeta (Fig. 3). We interpreted these 2D sections to assess the types and boundaries of various lithologies, and also to evaluate the subsurface extensions of the exposed mineralized quartz veins and associated alteration zones.

4. RESULTS

4.1. Geology of the Kestanelik Deposit Area

In total, eight rock units were defined in this study and these are, from the oldest to the youngest: mica schist, serpentinite, quartz-feldspar-hornblende (QFH) porphyry, calcareous sandstone, pyroclastics, andesite, basalt and colluvium (Fig. 2a). A generalized tectonostratigraphic section is given in Figure 2b. Major characteristics of the rock units are described below.

4.1.1. Rock units

Mica schist: The unit (Fig. 4a) covers one-fourth of the study

https://doi.org/10.1007/s12303-019-0030-y

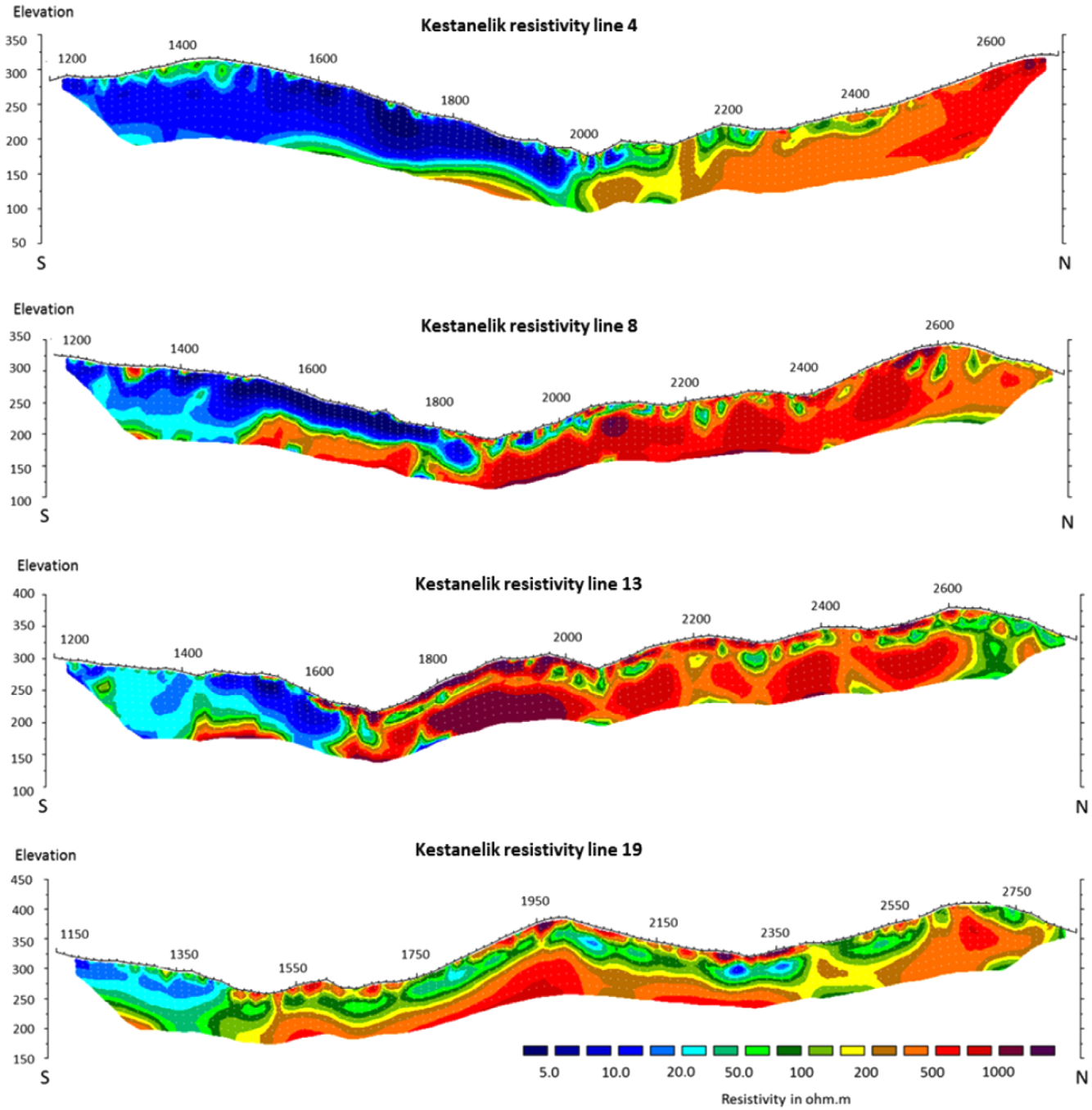

Fig. 3. Four of modeled 2D resistivity sections (From resistivity lines 4, 8, 13 and 19).

area and is mostly exposed in the central part (Fig. 2a). It belongs to the Paleozoic Çamlıca metamorphics and forms the local basement in the area. The schist predominantly contains biotite with lesser quartz and chlorite. The mica schist contains quartzite lenses, which are often oriented parallel to foliation (Fig. 4b).

Mica schist is in contact with serpentinite (Fig. 4c) in the central part of the study area but the contact between these two units is not well-exposed. The unit is cut by QFH porphyry north of Kestanelik River (Fig. 4d) and its contact with QFH porphyry was observed in a number of locations, where the foliation of schist changes, and the porphyry is brecciated along the contact. The mica schist unit is unconformably overlain by pyroclastics (Fig. 4e) along most of the Kestanelik River and by Quaternary colluvium (Fig. 4c) in the central part of the study area.

Whitish green serpentinite: The unit (Fig. 4c), represented by a small outcrop in the central part of the study area (Fig. 2a),

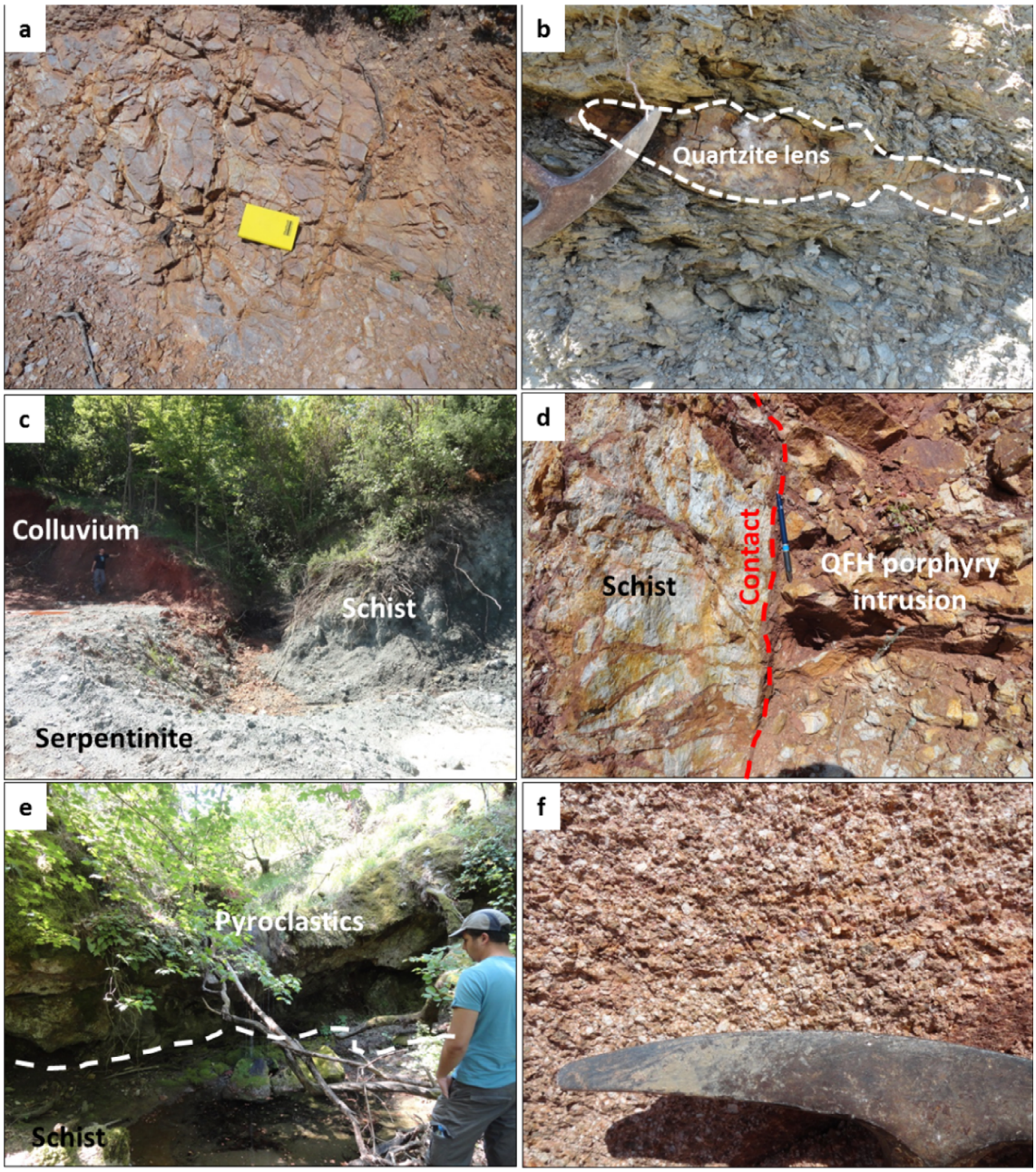

Fig. 4. (a) An outcrop of biotite ± quartz schist (481076m E, 4462556m N, Zone 35N). (b) A quartzite lens parallel to the foliation of the schist (482287m E, 4462389m N, Zone 35N). (c) Contacts of mica schist with serpentinite and colluvium (482379m E, 4462306m N, Zone 35N). (d) Contact of mica schist with QFH porphyry (481686m E, 4461493m N, Zone 35N). (e) Contact of mica schist with pyroclastics (481678m E, 4461418m N, Zone 35N). (f) Close up view of the QFH porphyry (482015m E, 4461691m N, Zone 35N).

belongs to the Çetmi ophiolitic mélange. It is unconformably overlain by Quaternary colluvium (Fig. 4c).

Quartz-feldspar-hornblende (QFH) porphyry: The unit (Fig. 4f) is represented by two N-S elongated bodies exposed in the central and north-eastern part of the study area (Fig. 2a). It contains coarse-grained quartz, feldspar and hornblende with minor biotite. Where the unit cuts mica schist it has a chilled and brecciated margin (Fig. 4d). The unit is also cut by some mafic dykes which are only observed in drill core (Fig. 5a). The unit most likely has a genetic link with the Northern Eocene age plutons which vary between ~48 and ~34 Ma due to its geographical proximity and similarity to dated plutons. Fresh plutonic rocks having mineralogical similarity with the QFH porphyry around the study area returned radiometric ages around ~45 Ma (Ercan et al., 1998; Delaloye and Bingöl, 2000) which can be accepted as the likely age of the unaltered QFH porphyry outcropping in the study area.

Calcareous sandstone: This unit (Fig. 5b) mostly crops out

https://doi.org/10.1007/s12303-019-0030-y

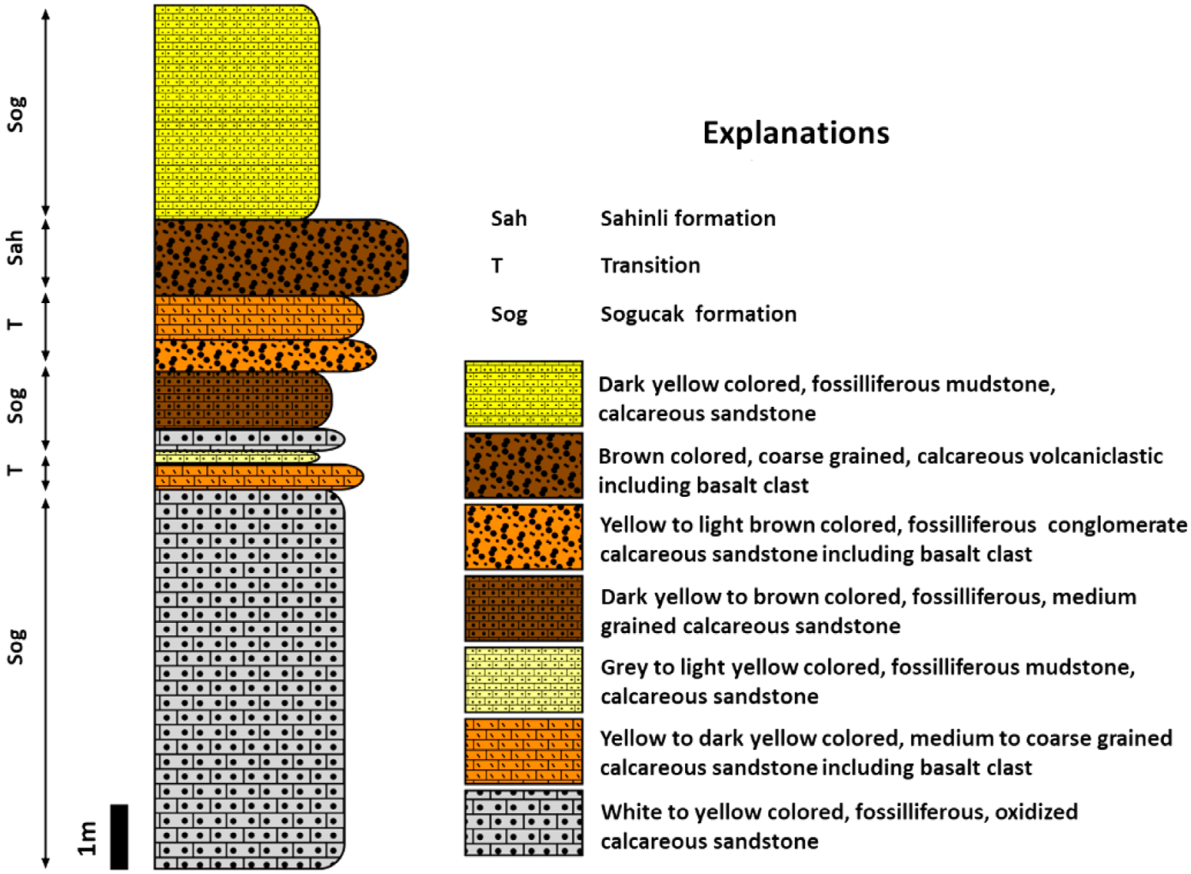

Fig. 5. Measured section showing the transition of the calcareous sandstone and the pyroclastics.

along the Kestanelik River in the southern part of the study area (Fig. 2a). It also has two small outcrops in the central and SE part of the area. It is characterized by white to pale yellow, medium-grained, thin- to medium-bedded, fossiliferous calcareous sandstone (Fig. 5b). The unit is likely to be part of the Soğucak formation. Nummulite fossils (Fig. 5b) indicate a shallow marine depositional environment, and an Eocene–Oligocene depositional age for this unit. According to a detailed study on the fossil assemblage collected from the unit, the age of the unit is suggested to be Priabonian (Late Eocene); (personal communication, Ercan Özcan, 2014). The unit is seen to be in lateral and vertical transition with the overlying pyroclastics at a location in the Kestanelik River (Figs. 5c and d) in the southern part of the study area and, a measured section for the boundary is given in Figure 5e.

Below the calcareous sandstone, there is a limited outcrop of basal conglomerate which is only observed at one location near the Kestanelik River (Fig. 6a). It contains sub-angular to rounded abundant clasts and boulders of vein quartz and lesser clasts and fragments of schist (Fig. 6b) ranging in size from 1 cm to 2 m. It is semi-lithified and appears to have been deposited in a high energy environment. Large boulders of mineralized quartz (up to 2 m) within the conglomerate contain anomalous gold values (> 20 g/t).

Andesitic to basaltic pyroclastics, basalt, and andesite: These three units mostly crop out south of Kestanelik River in the southern part of the study area (Dönmez et al., 2005). They are all geochemically associated and belong to the Şahinli Formation (Dönmez et al., 2005) for which the type locality (Şahinli Village) is 2 km from the study area. The pyroclastics are generally grey, poorly-sorted and include andesitic to basaltic clasts (Fig. 6c). Locally, they alternate with mudstones (Fig. 6d). These pyroclastics are intruded by both andesite and basalt dykes (Fig. 2a). Basalt (Fig. 6e) is exposed in the southwestern part of the area and is chloritized (Fig. 6f). Considering the transitional relationship of these units with the calcareous sandstone, their age should be close to Priabonian. This is consistent with the radiometric age (~37 Ma) obtained from the calc-alkaline volcanic rocks around Şahinli Village (Ercan et al., 1998; Delaloye and Bingöl, 2000).

Quaternary colluvium: The unit is exposed in limited areas along the Kestanelik River and in the eastern part of the study area. It is red, matrix-supported, poorly-sorted (clast sizes range between 0.5 cm and 20 cm) and includes angular to rounded clasts of mica schist, quartzite, QFH porphyry, and calcareous sandstone (Figs. 6g and h). Based on field observations, its maximum observed thickness is 60 m.

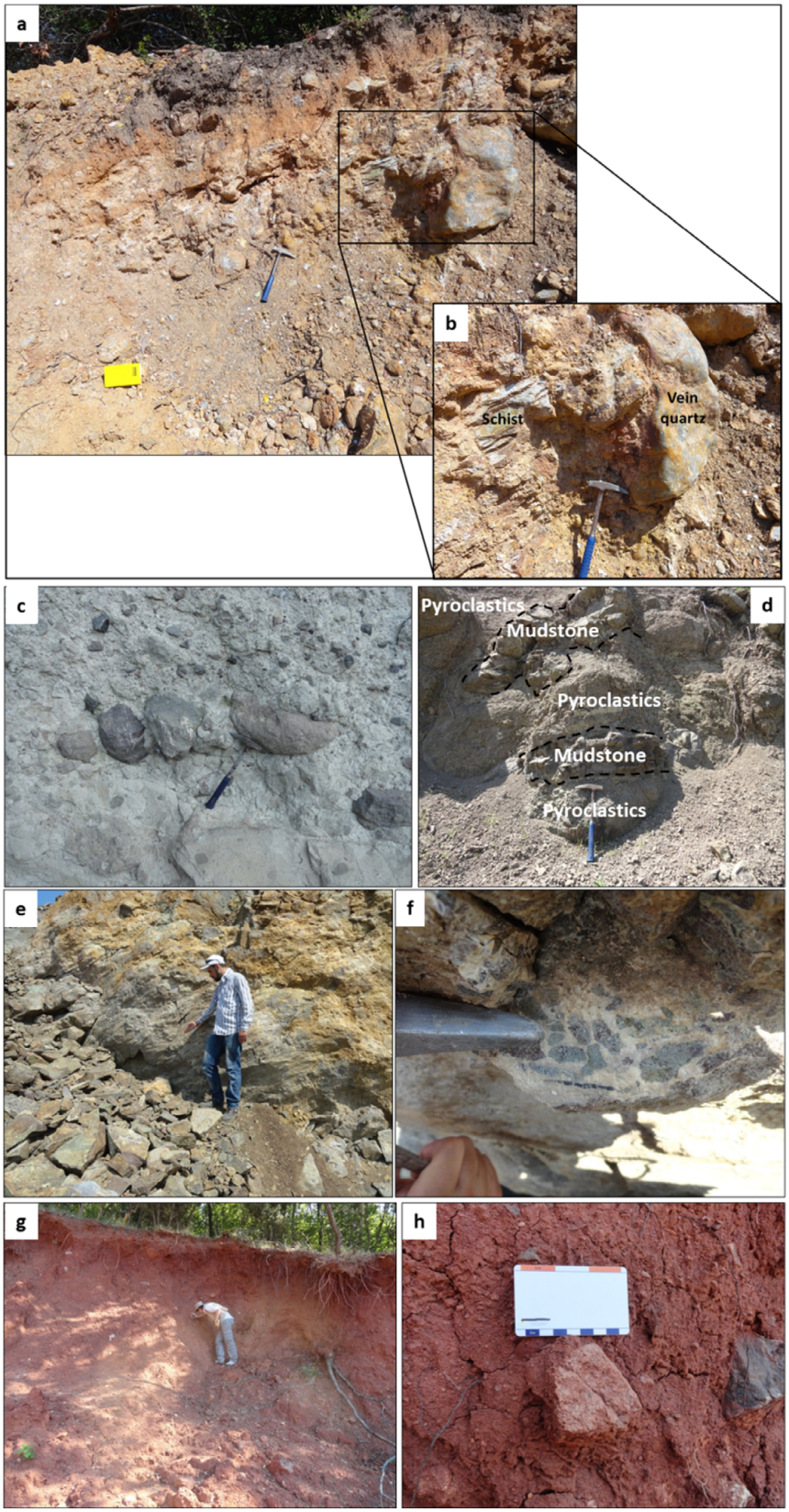

Fig. 6. (a) Basal conglomerate below the calcareous sandsone with sub-angular to rounded clasts of vein quartz and schist (481396m E, 4461698m N, Zone 35N). (b) Closer view of vein quartz and schist clasts. (c) An outcrop of andesitic to basaltic pyroclastics (480879m E, 4461492m N, Zone 35N). (d) Alternation of the pyroclastics with the mudstones (482139m E, 4461127m N, Zone 35N). (e) An outcrop of the altered basalt (480592m E, 4461224m N, Zone 35N). (f) Chloritization in the basalt (480592m E, 4461224m N, Zone 35N). (g) General view of the colluvium (482374m E, 4462308m N, Zone 35N). (h) Clasts observed in the colluvium (482374m E, 4462308m N, Zone 35N).

https://doi.org/10.1007/s12303-019-0030-y

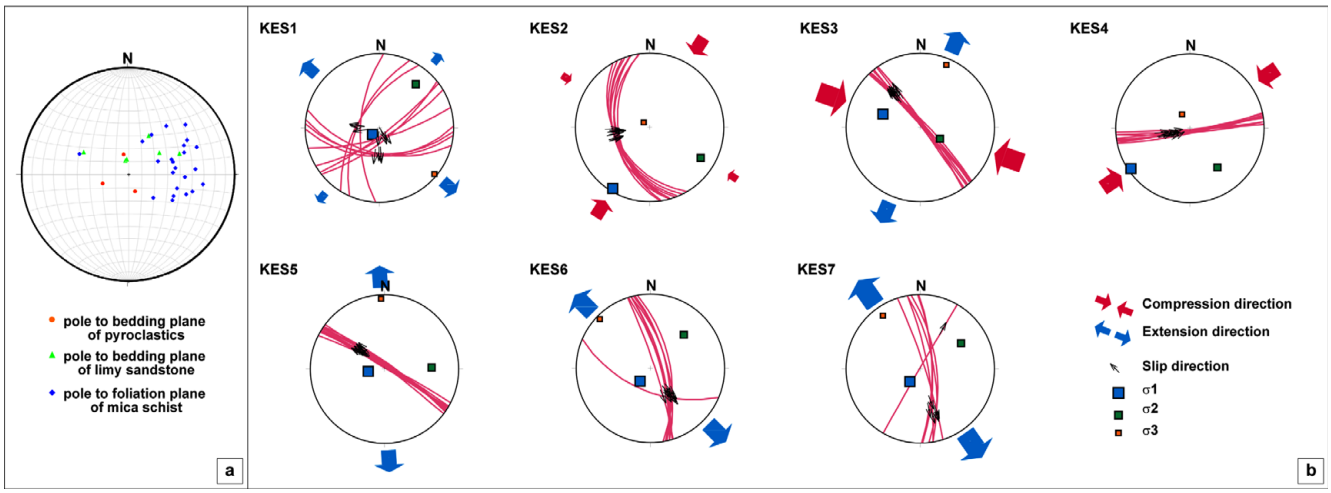

Fig. 7. (a) Poles to the foliation planes of mica schist and bedding planes of calcareous sandstone and pyroclastics plotted on an equal-area stereonet on the software Stereonet 9.5 (Allmendinger et al., 2013; Cardozo and Allmendinger, 2013). (b) Cyclographic traces, slickensides and constructed paleostress configurations of fault plane measurements from the Kestanelik area.

4.1.2. Structures

During geological mapping, attitude measurements were taken from foliation planes of schist and bedding planes of calcareous sandstone and pyroclastics. These data are shown on the geological map (Fig. 2a). Attitude measurements were recorded from fault planes together with the rake of slickenlines, and sense of slip (using surface geometry and/or offsets).

Strike direction of foliation planes in the schist (Fig. 7a) has a mean of 155° (n = 22). The mean dip of the foliation planes was calculated as 43° (n = 22). Due to limited access to the outcrops of the bedded calcareous sandstone and pyroclastics, structural data were collected from only 9 locations (3 from pyroclastics, 6 from calcareous sandstone). The bedding is different in the calcareous sandstone from the younger pyroclastics (Fig. 7a): the mean orientation of the bedding planes of the calcareous sandstone was calculated as 110°/29°, while that of the pyroclastics was calculated as 101°/17°.

4.2. Faults and Paleostress Analyses of Fault-slip Data

For each location, a minimum of 4 slip data are required to be processed in a paleostress analysis. In total 69 fault-slip data from 7 locations: KES1 to KES7 (Fig. 2a) were processed in T-TECTO 3.0 by considering the restrictions mentioned above. The results of paleostress analyses from these 7 locations are summarized in Table 1 and Figure 7b.

According to the paleostress inversion solutions together with field observations and (Φ') values, three different deformation regimes were determined. The first regime is represented by 2 sites (KES2 and KES4) (Fig. 2a) and show NE-SW-oriented compression with almost vertical σ_3. The second regime is represented by 4 sites (KES1, KES5, KES6 and KES7) (Fig. 2a) and indicates almost NW-SE oriented extension with σ_1 very close to vertical. The final regime is represented by the KES3 site and is determined as a pure-strike-slip regime developed under ESE-WNW-oriented compression and NNE-SSW-oriented extension.

4.3. General Characteristics of the Mineralization

The Kestanelik gold mineralization consists of epithermal quartz veins (Fig. 2a). The veins at Kestanelik generally shows open space filling and replacement textures represented by (1) crustiform, cockade (Figs. 8a and b), colloform, and (2) very common pseudo-bladed (Figs. 8c and d) and saccharoidal (Figs. 8d–f) quartz textures respectively. A diagnostic paleosurface feature of many low- and intermediate-sulphidation epithermal

Table 1. Results of paleostress analyses (see Fig. 2a for localities)

ID	σ_1	σ_2	σ_3	Φ	Φ'	n
KES1	226/76	040/14	130/1	0.1	0.1	11
KES2	211/02	121/12	310/78	0.8	2.8	9
KES3	289/34	120/56	023/05	0.3	1.7	11
KES4	236/02	145/24	330/66	0.7	2.7	9
KES5	262/65	088/25	357/03	0.3	0.3	10
KES6	219/65	045/25	314/03	0.4	0.4	9
KES7	219/65	058/24	325/08	0.6	0.6	10

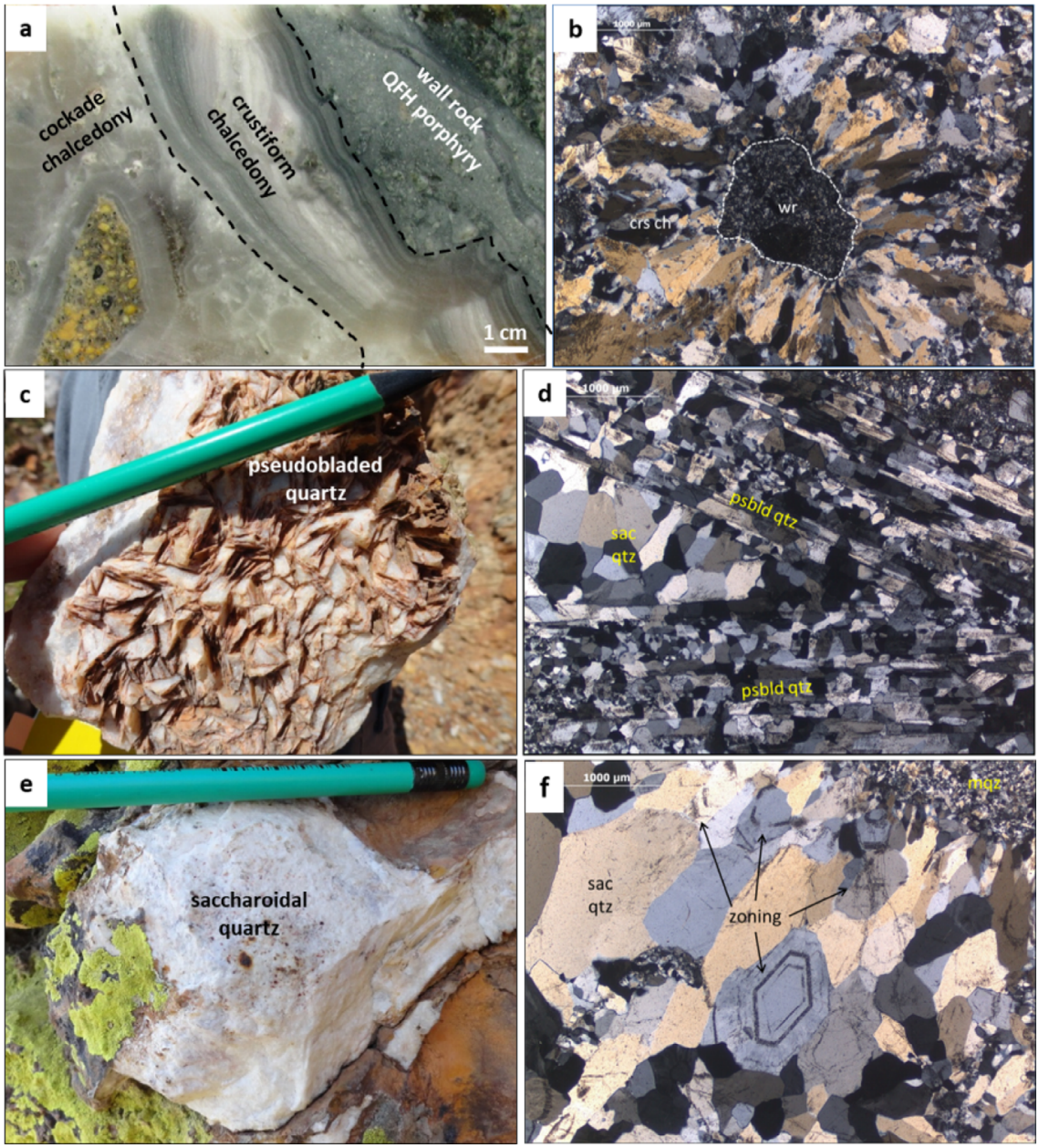

Fig. 8. (a) Cockade and crustiform chalcedony of the Karatepe vein in a drillcore of KED-16 at 124.2–124.4 m. (b) Crustiform chalcedony (crs ch) rimming a clast of altered wall rock QFH porphyry (wr) and forming the cockade texture at the Karatepe vein (crossed polars image from the thin section of KED-16 124 m). (c) Pseudobladed quartz replacing bladed calcite from the outcrop of KK2 vein (338 m asl). (d) Altered synchronous interstitial saccharoidal (sac qtz) and lattice bladed quartz (psbld qtz) at the K3 vein (crossed polars image from the thin section of a hand sample taken from the K3 vein outcrop). (e) Saccharoidal quartz observed on KK1 vein outcrop (318 m asl). (f) Zoned saccharoidal quartz crystals at the K3 vein (crossed polars image from the thin section of a hand sample taken from the K3 vein outcrop).

systems, amorphous silica sinter (Hedenquist et al., 2000), is absent at Kestanelik.

The most striking feature of the veins is brecciation. Quartz vein breccias are generally characterized by monomictic and polymictic hydrothermal breccias containing angular to sub-rounded clasts of host rocks and/or previous mineralized quartz veins cemented by (i) contemporaneous hematite and microcrystalline quartz (quartz-hematite cement; Fig. 9a) or (ii) contemporaneous goethite and microcrystalline quartz (Fig. 9b). The cores containing quartz-hematite and quartz-goethite cemented hydrothermal breccias have gold assay values up to ~60 g/t. However, it is not yet clear whether the high-grade gold is associated with the quartz-hematite matrix or quartz-goethite matrix or with earlier quartz vein clasts in the breccias.

Apart from the hematite and goethite cementing the breccias, hematite and dominantly goethite are also observed in some

https://doi.org/10.1007/s12303-019-0030-y

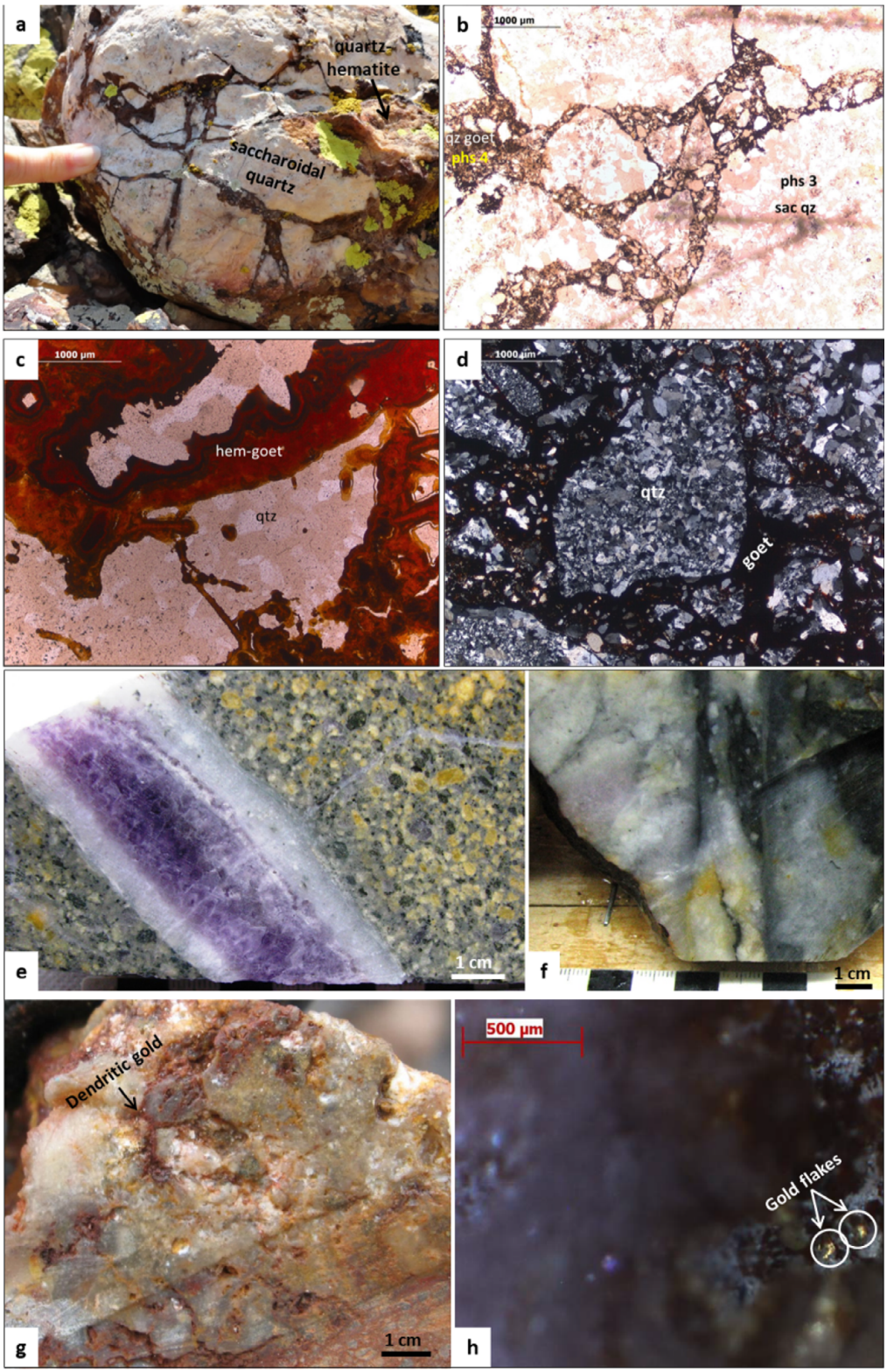

Fig. 9. (a) Hydrothermal crackle breccia with the clasts of saccharoidal quartz separated by quartz-hematite cement at the KK1 vein (320 m asl). (b) Hydrothermal mosaic breccia with angular to sub-rounded saccharoidal quartz (sac qz) clasts cemented by quartz-goethite (qz goet) at the KK1 vein (Plane polarized light image from the thin section of KED-7 13.1 m). (c) Colloform hematite and goethite (hem-goet) rimming the fractures cutting the crystalline quartz (qtz) at the K3 vein (Plane polarized light image from the thin section of KED-14 70.5 m). (d) Geothite filling the vugs and spaces between the crystalline quartz clasts and fragments at the K3 vein (Crossed polars image from the thin section of KED-14 70.6 m). (e) Crystalline amethystine quartz vein cutting QFH porphyry in drillcore KED-8 106.5 m, 0.081 g/t Au, 1980 ppm As. (f) Breccia with fine to coarse fragments of vein quartz cemented by gel quartz and fine pyrite in drillcore KED-2 46.8 m, 6.36 g/t Au. (g) Dendritic gold grains within the hematite cemented breccia. (h) Native gold flakes within the cavities infilled by goethite.

veins as (1) rimming and filling the post-mineral fractures (Fig. 9c), and (2) filling the vugs and spaces between the clasts and fragments (Fig. 9d). Related drill core intervals generally return gold grades up to 100 g/t and sometimes > 100 g/t.

Drill core assays of mineralized intervals indicate that quartz veins generally have moderate to high gold grades (Au range in 1–20 g/t) and low sulphide content (2–4% volume). Elevated values of silver (Ag) up to 85 g/t are associated with gold, and the Au:Ag ratio is generally in the range 2:1 to 1:2. The highest Au grade of 419 g/t was obtained from one channel sample taken from a narrow vein from the sheeted quartz veins in the valley floor.

4.4. Vein Mineralogy

4.4.1. Gangue mineralogy

The quartz veins principally consist of fine to medium grained quartz with minor fine-grained chalcedony (Figs. 8a and b). Crustiform and colloform banded chalcedony are only observed at the Karatepe vein in the northern third of the study area. It is poor in gold and is associated with low gold grades having a mean of 0.52 g/t. By contrast, other veins are dominated by crypto- to micro-crystalline saccharoidal quartz (Figs. 8e and f) replacing massive granular calcite which is associated with gold grades up to ~4 g/t. Another carbonate-replacement texture pseudo-bladed quartz replacing bladed calcite (Figs. 8c and d) is observed locally in the veins. Colloform banding is not common and commonly restricted to the K3 vein. At depth, some veins are associated with Au-poor crystalline amethystine quartz with As-rich material (pyrite?) confined to the QFH porphyry (Fig. 9e). A very common gangue mineral in LS systems, adularia, was not observed in the area. The veins are very sulphide poor (2–4% volume). Pyrite is the only sulphide associated with the mineralization. It is not particularly widespread and is finely disseminated in the breccia matrix and some of the quartz vein material (Fig. 9f).

4.4.2. Ore mineralogy

Ore minerals are native gold and accessory native silver. Most of the gold is microscopic. Very limited gold grains are visible and are only observed where the veins contain bonanza grades > ~60 g/t (Fig. 9g). Microscopic gold is seen as dendritic pale-coloured native gold flakes within (1) the hematite cemented breccia and (2) cavities infilled by goethite (Fig. 9h). However, it is common and hosted by goethite-rich vein samples. No other metal anomalies except silver are associated with gold. The Kestanelik deposit has being operated as an active open-pit mine for precious metals gold and silver since November 2017 (personal communication, Cem Yüceer, 2019). Arsenic (As) concentrations are slightly elevated, although are generally below 250 ppm.

4.5. General Characteristics of the Hydrothermal Alteration

The alteration mineral paragenesis has been obtained by Portable Infrared Mineral Analyzer (PIMA) analyses conducted from the host rocks on the surface and drill core samples. PIMA analyses showed that the altered rocks consist commonly of illite, smectite, sericite with lesser pyrite. Besides, iron-oxides including hematite and goethite, and relatively rare calcite were also detected by the PIMA analyses from the mineralized quartz veins. The alteration types and terminology was defined based on the predominant paragenetic minerals in the altered rocks.

Hydrothermal alteration is more pervasive within the QFH porphyry host, and is weak or very limited to any discernible extent within the schist in the field. The alteration is composed of clays mostly illite and interlayered illite/smectite in composition, suggesting that the alteration is of intermediate argillic alteration type (Fig. 10a). Pervasive strong illite alteration of feldspars in the QFH porphyry is highly remarkable. Smectite is observed, particularly in the northern part of the study area around the Karatepe vein near the surface. Propylitic alteration consisting mainly of chlorite and pyrite is also identified distal to the veins in the marginal zone on the north-eastern outcrop of the QFH porphyry (Fig. 10b). Fine grained euhedral–subhedral crystals of sericite replacing muscovite in the mica schist were observed locally around the KK1 and KK2 veins (Fig. 10c). In the northern part of the study area, variably silicified rocks occur as resistant silica ledges (Fig. 10d) which have halos of swelling clays within a few meters, mostly smectite.

Correlation coefficients (r^2 values varying between 0.2 and 0.7) calculated using drill core and RC assay data of altered host rocks show that Al is weakly to strongly positively correlated with Ca, Mg, Na and some clay group elements like Fe, K and Ti.

5. DISCUSSION

5.1. Formation of the Kestanelik Epithermal Gold Deposit in the Geological Context of the Biga Peninsula

Within the Biga Peninsula, the Paleozoic metamorphic and ophiolitic basement rocks are cut by Eocene–Miocene plutons and are also covered by Cenozoic volcanic and sedimentary units. Starting from the Eocene, extensive syn- to post-collisional magmatism prevailed in NW Turkey, which shifted from calc-alkaline to alkaline character in the middle–late Miocene (Dilek and Altunkaynak, 2006; Altunkaynak and Genç, 2008). Basement

https://doi.org/10.1007/s12303-019-0030-y

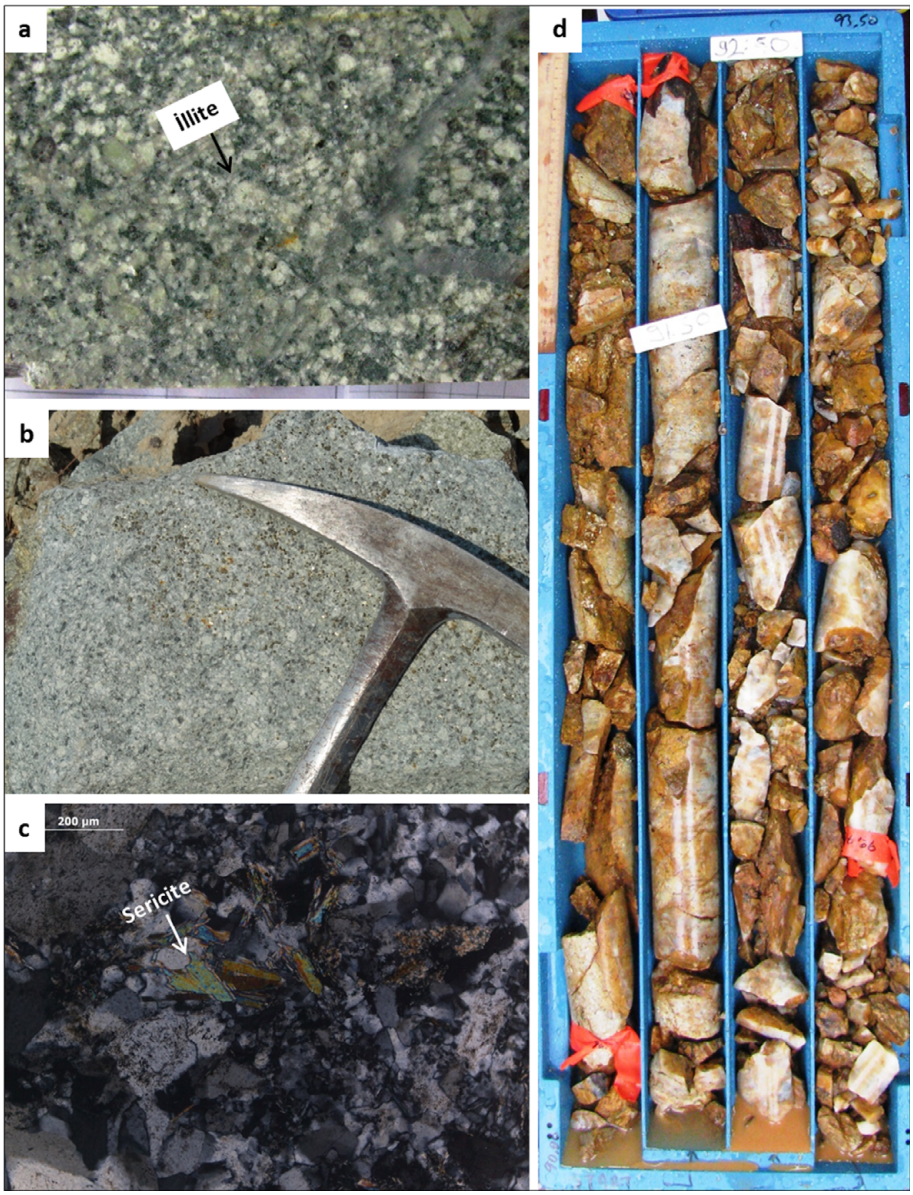

Fig. 10. (a) Pervasive illite alteration of feldspars in the QFH porphyry around the Karatepe vein in drillcore KED-16 80.7 m. (b) Propylitic alteration in the form of chlorite and pyrite distal to the veins on the north-eastern outcrop of the QFH porphyry (484307 m E, 4461839 m N, Zone 35N). (c) Muscovite in the mica schist transformed to sericite as a result of alteration (Crossed polars image from the thin section of a hand sample taken from the outcrop of KK1 vein). (d) Silicified zone around the Karatepe vein at KED-21 90–93.5 m.

rocks consisting of Paleozoic mica schists of the Çamlıca metamorphics and obducted serpentinites of the Çetmi Ophiolitic melange are intruded by QFH porphyry, and are underlain by the volcanic and sedimentary units of the area. Calcareous sandstone of the Soğucak formation is in lateral and vertical transition with volcaniclastics of the Şahinli formation in the area (Fig. 5e), although Yüzer and Tunay (2012) states that the Soğucak formation is also overlain by the Şahinli formation, indicating that volcanism causing the deposition of Şahinli Formation started in the area while marine deposition was still active.

Gold mineralization in the Kestanelik deposit is associated with quartz veins/breccias hosted by Paleozoic mica schist and Lutetian QFH porphyry. Limestone and pyroclastics neither host quartz veins nor show any hydrothermal alteration, implying that they postdate mineralization. In addition, the basal conglomerate (Fig. 6a) below the calcareous sandstone has the clasts and boulders of mineralized Au-rich quartz veins indicating that the calcareous sandstone is younger than the mineralization. There is a noticeable break in the 2D resistivity sections (Fig. 3) along the Kestanelik River at the lithological boundary separating the high resistivity domains of the mineralized area (silicification zone) in the north (represented by warm red-purple-orange colours) from the low resistivity domains of sedimentary and volcanic units in the south (represented by cold blue-green colours) (Fig. 3). Although, this may be indicative of a possibility that the units south of the river are neither altered nor mineralized, the drilling campaign along with geophysical surveys enabled the discovery of buried quartz veins/breccia bodies with the same direction

under the sedimentary cover. A gently-doming to flat-lying high resistivity layer (observed on lines 8 to 19 on Fig. 3) below the low resistivity layer at the south of the river (Fig. 3) could correspond to a flat-lying, mineralised-silicified zone hosted by schist or intrusive rocks overlain by volcano-sedimentary units. This is interpreted to be due to boulders and large clasts of silicified rocks and veins within the basal conglomerate, and the drilling also revealed that the basal conglomerate and buried quartz veins/breccia bodies are also economically mineralized, and will be included in the mining operations at the deposit. This horizon is overlain by Priabonian calcareous sandstone, the oldest unit covering the mineralized veins. On the other hand, the youngest host rock to the mineralized quartz veins is QFH porphyry which is middle Lutetian in age. The stratigraphic age of the mineralization must therefore be middle Lutetian–early Priabonian. However, a more precise age would be obtained by dating the mineralized veins.

Although the host rock porphyry was thought to be the heat source for the epithermal system by some geologists, this is unlikely because the coarse grain size of the porphyry matrix shows that it was probably emplaced at a greater depth (sub-volcanic level) and then uplifted and eroded before a mineralization style characteristic of much shallower depths occurred. For this reason, there must have been a younger intrusion below the mineralized quartz vein system to provide the heat source. Based on the timing of the mineralization (middle Lutetian–early Priabonian), the heat source most likely has a genetic link with the Cenozoic post-collisional calc-alkaline magmatism prevailing in the Biga Peninsula. There are several high-sulphidation (e.g., Kuşçayırı, Kartaldağ) and low sulphidation (e.g., Madendağ, Adatepe) epithermal deposits yielding similar ages to the Kestanelik (between 43–34 Ma based on Ar/Ar dating analyses; Yiğit, 2012; Ünal-İmer et al., 2013) deposit with the Biga Peninsula. Because Kestanelik and these late Eocene epithermal deposits in the region seem to have a genetic and temporal relationship with the Cenozoic magmatism, the Late Eocene is seen as an important metallogenic epoch related to the regional Tethyan metallogeny. However, this could be fully supported by precise geochronology of the alteration at Kestanelik by (U + Th)/He dating on hypogene hematite (e.g., Wernicke and Lippolt, 1997) in the veins where adularia is absent to be dated by Ar/Ar geochronology.

From fault paleostress inversion solutions and with field observations, three different deformation regimes were determined: (1) NE-SW-oriented compression, (2) NW-SE-oriented extension and (3) a pure-strike-slip regime developed under ESE-WNW-oriented compression and NNE-SSW-oriented extension (Fig. 7b). Providing time constraints is not possible for each regime as no growth fault and/or sealing units exist. However, the first two deformation regimes may belong to a single deformation phase, because a NE-SW-oriented compressional regime (first regime) could also cause NW-SE oriented extension (second regime). In this case, the pure-strike-slip regime cutting the youngest unit of the area constitutes the second deformation phase in the study area. The first deformation phase is likely due to the collision and further convergence after the closure of the northern branch of the Neo-Tethys Ocean along the İAESZ in NW Turkey in the late Cretaceous–early Eocene (Şengör and Yılmaz, 1981; Harris et al., 1994; Okay and Tüysüz, 1999; Sherlock et al., 1999; Önen and Hall, 2000; Hinsbergen et al., 2010). The inferred directions of the principal stresses determined by kinematic analysis of the mineralized vein system, almost NE-SW oriented sub-horizontal compression (Gülyüz et al., 2018), is consistent with the first deformation phase contemporaneous with mineralization. Thus, it is inferred that the NE-SW oriented compressional regime and associated tectonism is responsible for the formation and reactivation of the structural network that provided pathways for the circulation of the hydrothermal fluids. The second phase is likely related to the present-day trans-tensional neotectonic regime characterized by the splays of North Anatolian Fault Zone in NW Turkey (Kaymakcı et al., 2007).

5.2. Mineralization at the Kestanelik Epithermal Gold Deposit

The gold mineralization in the area is of low-sulphidation epithermal type, as evidenced by some diagnostic features of LS epithermal deposits: hydrothermal breccia, bladed quartz replacing bladed calcite (pseudobladed quartz), and also the low total sulphide (2–4%) and base metal contents in the veins. However, the very common and diagnostic gangue mineral in LS systems adularia, is absent at Kestanelik. The absence of adularia can be attributed to the calc-alkaline host rock because adularia rarely occurs when there is not enough potassium in the wall rock. Alternatively, (i) fluid pH may have been below the adularia stability field (Thompson et al., 1994), (ii) temperature of fluids may have not been high enough for the formation of adularia, (iii) oxygen fugacity of the fluid may have been low (relatively less oxidizing fluid) or (iv) adularia may have been replaced by late illite (Simpson and Mauk, 2007). Absence of silica sinter, the diagnostic paleosurface indicator of LS epithermal systems, implies that the epithermal system must have been subjected to erosion, and that only the subsurface parts of the vein system are presently exposed at Kestanelik.

The most remarkable feature of the veins is brecciation (Figs. 9a–d). Quartz vein breccia and textural characteristics indicate that at least two phases of mineralization occurred in the area. Each brecciation event seems to have triggered rapid boiling of hydrothermal fluids by sudden pressure release evident from

https://doi.org/10.1007/s12303-019-0030-y

the diagnostic boiling indicators: lattice bladed quartz replacing calcite, colloform and crustiform textures and hydrothermal breccias. However, the absence of late stage brecciation which is characterized by the hematite/goethite-quartz cementing hydrothermal breccias (Figs. 9a and b) at the deepest vein intercepts (–45 m RL) suggest that the process may have been effective only on approach to a paleosurface.

Common occurrence of pseudobladed quartz and saccharoidal quartz (Figs. 8c–f) observed in earlier stages of mineralization within the Kestanelik vein system shows that the hydrothermal fluid had high CO_2 content which was lost to the vapor phase and resulted in a pH increase and saturation of CO_3 leading to the deposition of bladed calcite and massive granular calcite, which were then dissolved (evident from their porous appearance) by a decrease in temperature upon boiling and pseudomorphed by quartz. In contrast, the youngest phase of the mineralization (hematite/goethite-quartz cementing the clasts) is associated with crystalline quartz, indicating silica-saturated hydrothermal fluid. Change of texture from pseudomorphs of calcite to crystalline quartz suggests the evolution of hydrothermal fluids from carbonate-saturated to silica-saturated.

Hematite and goethite together with crystalline quartz as cement to the hydrothermal crackle-mosaic breccias (Figs. 9a and b) are identified by petrographical analysis, and are synchronous with silicification of the breccias implying hypogene oxidation/mixing by oxidized fluids. Hypogene hematite and goethite thus suggest the mixing of ascending hydrothermal fluids with oxidized meteoric groundwater in the final stage of the mineralization. Hematite and goethite are also observed as (i) filling the fractures and (ii) filling some vugs between the clasts and fragments (Figs. 9c and d), and suggest supergene oxidation. These supergene iron oxides may have been precipitated during later processes that possibly leached the pyrite bearing quartz veins as a result of the infiltration of meteoric water into the post-mineral fractures and vugs. Since boiling-related textures and both hypogene and supergene hematite and goethite are associated with gold; boiling, mixing and supergene enrichment can each be suggested as gold precipitation mechanisms in the Kestanelik veins. However, the common presence of gold within the supergene hematite and goethite (Figs. 9g and h) and their association with gold grades up to and more than 100 g/t indicate that the gold grades were elevated by supergene enrichment process.

Because especially Al, Ti and K are resistant to chemical dissolution indicating precipitation by clays, the positive relationship of Al with Ca, Fe, K, Mg, Na and Ti could be attributed to the presence of illite and interlayered illite/smectite. Their presence characterizes the argillic alteration created by mildly acidic (pH 4–5) water generated by CO_2-rich steam-heated water in the margins of the mineralized veins. Minerals detected during the PIMA analyses also support the observed alteration minerals in the area as well as the hypogene and supergene oxidation products hematite and goethite.

6. CONCLUSIONS

The study presented in this paper has found the following:

- The mineralization in Kestanelik is associated with major quartz veins, sheeted quartz veins in the valley and wall rock veins surrounding the major quartz veins, which are hosted by middle Lutetian QFH porphyry and Paleozoic mica schist.
- The host rock porphyry is not the heat source for the epithermal system: there must be a younger intrusion below the mineralized vein system which provided the necessary heat for the circulation of the hydrothermal fluids.
- The mineralization is low sulphidation epithermal type evident from pseudo-bladed quartz, colloform to crustiform quartz, and comb to cockade vein textures, hydrothermal breccias and total low sulphide and base metal contents.
- Native gold and silver are the ore minerals, while the quartz (the most dominant one), chalcedony, calcite and disseminated pyrite are the gangue minerals at Kestanelik. However, the common gangue adularia in LS systems is absent.
- There are at least two phases of mineralization at Kestanelik. Textural and mineralogical characteristics of the veins indicate the evolution of hydrothermal fluids from carbonate- to silica-saturated.
- Boiling, mixing (hypogene oxidation) and supergene enrichment (supergene oxidation) are the prevailing mechanisms of gold precipitation. However supergene enrichment elevated the gold content, resulting in gold grades up to and more than 100 g/t.
- Hydrothermal alteration is especially conspicuous around the veins in the porphyry host, and is commonly represented by intermediate argillic alteration.
- The age of the mineralization, bracketed by cross cutting relations and supported by resistivity data, is middle Lutetian–Early Priabonian.
- Based on the timing of the mineralization (Late Eocene), the heat source most likely has a genetic link with the Cenozoic post-collisional calc-alkaline magmatism prevailing in the Biga Peninsula.
- Paleostress inversion solutions from faults compared to those for the mineralised veins indicate two different tectonic regimes: (1) NE-SW oriented compression and (2) strike-slip regime developed under ESE-WNW oriented compression and NNE-SSW oriented extension. The first one is attributed to the collision and further convergence after the closure of the northern branch of the Neo-Tethys Ocean along the İAESZ in NW Turkey in the Late Cretaceous–Early Eocene and

associated tectonism is responsible for the formation and reactivation of the structural network which provided pathways to the circulation of the hydrothermal fluids. The second one is related to the present-day trans-tensional neotectonic regime characterized by the splays of North Anatolian Fault Zone in NW Turkey.

ACKNOWLEDGMENTS

This study was a part of a PhD project carried out at the University of Strathclyde with a University of Strathclyde scholarship and financial support from Geochemico Incorporated. The study benefited from discussions with Nuretdin Kaymakcı. We thank Ali İmer for his valuable comments on the earlier version of the manuscript. The authors are grateful to Chesser Resources for providing accommodation and logistics for fieldwork, and access to the drill hole, geochemistry and geophysical data. We also thank C. S. Yüceer, M. Çetintas, and geologists and staff at the Kestanelik for their generous help in all phases of the fieldwork. Finally, I appreciate the late David. R. Gladwell for providing financial support from the Geochemico Incorporated and help during the fieldwork. His memory will be with me always.

REFERENCES

Allmendinger, R.W., Cardozo, N.C., and Fisher, D., 2013, Structural Geology Algorithms: Vectors and Tensors. Cambridge University Press, Cambridge, 289 p.

Altunkaynak, Ş. and Genç, Ş.C., 2008, Petrogenesis and time-progressive evolution of the Cenozoic continental volcanism in the Biga Peninsula, NW Anatolia (Turkey). Lithos, 102, 316–340.

Angelier, J., 1979, Determination of mean principal direction of stress for a given fault population. Tectonophysics, 56, 17–26.

Angelier, J., 1989, From orientation to magnitudes in paleostress determinations using fault slip data. Journal of Structural Geology, 11, 37–50.

Angelier, J., 1994, Fault slip analysis and paleostress reconstruction. In: Hancock, P.L. (ed.), Continental Deformation. Pergamon Press, Oxford, p. 53–101.

Armijo, R., Carey, E., and Cisternas, A., 1982, The inverse problem in microtectonics and the separation of tectonic phases. Tectonophysics, 82, 145–160.

Beccaletto, L., Bartolini, A.C., Martini, R., Hochuli, P.A., and Kozur, H., 2005, Biostratigraphic data from Çetmi Melange, northwest Turkey: palaeogeographic and tectonic implications. Palaeogeography, Palaeoclimatology, Palaeoecology, 221, 215–244.

Bozkurt, E., 2001, Neotectonics of Turkey – a synthesis. Geodinamica Acta, 14, 3–30.

Cardozo, N. and Allmendinger, R.W., 2013, Spherical projections with OSX Stereonet. Computers & Geosciences, 51, 193–205.

Cavazza, W., Okay, A.I., and Zattin, M., 2009, Rapid early-middle exhumation of the Kazdağ Massif (Western Anatolia). International Journal of Earth Science, 98, 1935–1947.

Delaloye, M. and Bingöl, E., 2000, Granitoids from western and northwestern Anatolia: geochemistry and modeling of geodynamic evolution. International Geology Reviews, 42, 241–268.

Delvaux, D., Moeys, R., Stapel, G., Petit, C., Levi, K., Miroshenko, A., Ruzhıch, V., and Sankov, V., 1997, Paleostress reconstructions and geodynamics of the Baikal region, Central Asia, Part 2. Cenozoic rifting. Tectonophysics, 282, 1–38.

Dönmez, M., Akçay, A.E., Genç, C., and Acar, Ş., 2005, Middle–Upper Eocene volcanism and marine ignimbrites of Biga Peninsula. Bulletin of Mineral Research and Exploration, 131, 49–61. (in Turkish with English abstract)

Ercan, T., Satir, M., Steinitz, G., Dora, A., Sarifakioglu, E., Adis, C., Walter, H.J., and Yildirim, T., 1998, Features of Tertiary volcanism around the Sea of Marmara. Bulletin of Mineral Research and Exploration, 120, 97–118. (in Turkish with English abstract)

Etchecopar, A., Vasseur, G., and Daigniers, M., 1981, An inverse problem in microtectonics for the determination of stress tensors from fault striation analysis. Journal of Structural Geology, 3, 51–65.

Gülyüz, N., Shipton, Z.K., Kuşcu, İ., Lord, R.A., Kaymakcı, N., Gülyüz, E., and Gladwell D.R., 2018, Repeated reactivation of clogged permeable pathways in epithermal gold deposits: Kestanelik epithermal vein system, NW Turkey. Journal of the Geological Society, 175, 509–524.

Hardcastle, K.C., 1989, Possible paleostress tensor configurations derived from fault-slip data in eastern Vermont and western New Hampshire. Tectonics, 8, 265–284.

Harris, N.B.W., Kelley, S., and Okay, A.I., 1994, Post-collision magmatism and tectonics in northwest Anatolia. Contributions to Mineralogy and Petrography, 117, 241–251.

Hinsbergen, D.J.J., Kaymakcı, N., Spakman, W., Torsvik, T.H., and Amaru, M., 2010, Reconciling geological history with mantle structure in western Turkey. Earth and Planetary Science Letters, 297, 674–686.

Kaymakcı, N., Aldanmaz, E., Langereis, C., Spell, T.L., Gurer, O.F., and Zanetti, K.A., 2007, Late Miocene transcurrent tectonics in NW Turkey: evidence from Paleomagnetism and ^{40}Ar-^{39}Ar dating of alkaline volcanic rocks. Geological Magazine, 144, 379–392.

Le Pichon, X. and Angelier, J., 1979, The Hellenic arc and trench system: a key to the neotectonic evolution of the eastern Mediterranean area. Tectonophysics, 60, 1–42.

Mckenzie, D.P., 1978, Active tectonics of the Alpine-Himalayan Belt: the Aegean Sea and surroundings regions (tectonics of the Aegean Region). Geophysical Journal International, 55, 217–254.

Meulenkamp, J.E., Wortel, W.J.R., Van Wamel, W.A., Spakman, W., and Hoogerduyn, S.E., 1988, On the Hellenic subduction zone and geodynamic evolution of Crete in the late middle Miocene. Tectonophysics, 146, 203–215.

Nemcok, M., Kovac, D., and Lisle, R.J., 1999, A stress inversion procedure for polyphase calcite twin and fault/slip data sets. Journal of Structural Geology, 21, 597–611.

Okay, A.I. and Tüysüz, O., 1999, Tethyan sutures of northern Turkey. In: Durand, B., Jolivet, L., Horváthand, F., and Séranne, M. (eds.), The Mediterranean Basins: Tertiary Extension within the Alpine

 https://doi.org/10.1007/s12303-019-0030-y

Orogeny. Geological Society, London, Special Publications, 156, p. 475–515.

Okay, A.I. and Satır, M., 2000a, Upper Cretaceous eclogite facies metamorphic rocks from the Biga Peninsula, northwest Turkey. Turkish Journal of Earth Sciences, 9, 47–56.

Okay, A.I. and Satır, M., 2000b, Coeval plutonism and metamorphism in a latest Oligocene metamorphic core complex in Northwest Turkey. Geological Magazine, 137, 495–516.

Okay, A.I., Siyako, M., and Bürkan, K.A., 1990, Geology and tectonic evolution of the Biga Peninsula. Bulletin of the Turkish Association of Petroleum Geologists, 2, 83–121. (in Turkish with English abstract)

Okay, A.I., Satır, M., Maluski, H., Siyako, M., Monie, P., Metzger, R., and Akyüz, S., 1996, Paleo- and Neo-Tethyan events in northwest Turkey: geological and geochronological constraints. In: Yin, A. and Harrison, M. (eds.), Tectonics of Asia. Cambridge University Press, Cambridge, p. 420–441.

Önen, A.P. and Hall, R., 2000, Subophiolite metamorphic rocks from NW Anatolia, Turkey. Journal of Metamorphic Geology, 18, 483–495.

Sanematsu, K., Duncan, R., İmai, A., and Watanabe, K., 2005, Geochronological constraints using $^{40}Ar/^{39}Ar$ dating on the mineralization of the Hishikari epithermal gold deposit, Japan. Resource Geology, 55, 249–266.

Sherlock, S., Kelley, S., Inger, S., Harris, N., and Okay, A.I., 1999, ^{40}Ar-^{39}Ar and Rb/Sr geochronology of high-pressure metamorphism and exhumation history of the Tavsanli Zone, NW Turkey. Contributions to Mineralogy and Petrology, 137, 46–58.

Simpson, M.P. and Mauk, J.L., 2007, The Favona epithermal gold-silver deposit, Waihi, New Zealand. Economic Geology, 102, 817–839.

Şengör, A.M.C. and Yılmaz, Y., 1981, Tethyan evolution of Turkey: a plate tectonic approach. Tectonophysics, 75, 181–241.

Thompson, J.F.H., Abidin, H.Z., Both, R.A., Martosuroyo, S., Rafferty, W.J., and Thompson, A.J.B., 1994, Alteration and epithermal mineralization in the Masupa Ria volcanic center, central Kalimantan, Indonesia. Journal of Geochemical Exploration, 50, 429–456.

Türkecan, A. and Yurtsever, A., 2002, Geological report of the İstanbul Sheet (1:500,000). General Directorate of Mineral Research and Exploration, Ankara, 27 p.

Ünal-İmer, E., Gulec, N., Kuscu, I., and Fallick, A.E., 2013, Genetic investigation and comparison of Kartaldag and Madendag epithermal gold deposits in Canakkale, NW Turkey. Ore Geology Reviews, 53, 204–222.

Wernicke, R.S. and Lippolt, H.J., 1997, Evidence of Mesozoic multiple hydrothermal activity in the basement at Nonnenmattweiher (southern Schwarzwald), Germany. Mineralium Deposita, 32, 197–200.

Yiğit, Ö., 2009, Mineral deposits of Turkey in relation to Tethyan metallogeny: implications for future mineral exploration. Economic Geology, 104, 19–51.

Yiğit, Ö., 2012, A prospective sector in the Tethyan Metallogenic Belt: geology and geochronology of mineral deposits in the Biga Peninsula, NW Turkey. Ore Geology Reviews, 46, 118–148.

Yüzer, E. and Gürkan, T., 2012, Biga Yarımadası'nın Genel ve Ekonomik Jeolojisi. Publication of the General Directorate of the Mineral Research and Exploration, Ankara, 326 p. (in Turkish with English abstract)

Žalohar, J. and Vrabec, M., 2007, Paleostress analysis of heterogeneous fault-slip data: the Gauss method. Journal of Structural Geology, 29, 1798–1810.